Ceramide-1-phosphate transfer protein promotes sphingolipid reorientation needed for binding during membrane interaction

Yong-Guang Gao[1]*, **Jeffrey McDonald**[1], **Lucy Malinina**[1], **Dinshaw J. Patel**[2], and **Rhoderick E. Brown**[1]*

[1]Hormel Institute, University of Minnesota, Austin, MN, USA; and [2]Structural Biology Program, Memorial Sloan Kettering Cancer Center, New York, NY, USA

Abstract Lipid transfer proteins acquire and release their lipid cargoes by interacting transiently with source and destination biomembranes. In the Glyco-Lipid Transfer Protein (GLTP) superfamily, the two-layer all-α-helical GLTP-fold defines proteins that specifically target sphingolipids (SLs) containing either sugar or phosphate headgroups via their conserved but evolutionarily-modified SL recognitions centers. Despite comprehensive structural insights provided by X-ray crystallography, the conformational dynamics associated with membrane interaction and SL uptake/release by GLTP superfamily members have remained unknown. Herein, we report insights gained from molecular dynamics (MD) simulations into the conformational dynamics that enable ceramide-1-phosphate transfer proteins (CPTPs) to acquire and deliver ceramide-1-phosphate (ClP) during interaction with 1-palmitoyl-2-oleoyl phosphatidylcholine bilayers. The focus on CPTP reflects this protein's involvement in regulating pro-inflammatory eicosanoid production and autophagy-dependent inflammasome assembly that drives interleukin (IL-1β and IL-18) production and release by surveillance cells. We found that membrane penetration by CPTP involved α-6 helix and the α-2 helix N-terminal region, was confined to one bilayer leaflet, and was relatively shallow. Large-scale dynamic conformational changes were minimal for CPTP during membrane interaction or ClP uptake except for the α-3/α-4 helices connecting loop, which is located near the membrane interface and interacts with certain phosphoinositide headgroups. Apart from functioning as a shallow membrane-docking element, α-6 helix was found to adeptly reorient membrane lipids to help guide ClP hydrocarbon chain insertion into the interior hydrophobic pocket of the SL binding site. 🔓 These findings support a proposed 'hydrocarbon chain-first' mechanism for ClP uptake, in contrast to the 'lipid polar headgroup-first' uptake used by most lipid-transfer proteins.

Nonvesicular sphingolipid (SL) trafficking in cells is mediated by lipid-transfer proteins (LTPs) that acquire and release their specific SL cargoes via transient interaction with source and destination biomembranes. In the GlycoLipid Transfer Protein (GLTP) superfamily, two families of cytosolic proteins exist that target ceramide-based SLs containing either phosphate or sugar headgroups. Phosphate headgroup SL-specific family members include human ceramide-1-phosphate (ClP) transfer protein (CPTP; 2l4 a.a.) and the plant CPTP ortholog, ACDll (206 a.a.); whereas glyco-headgroup SL-specific members include human GLTP (209 a.a.), fungal HET-C2 (208 a.a.), and human phosphatidylinositol-4-phosphate adapter protein-2 (FAPP2; 519 a.a.). Divergent evolutionary modifications to the two-layer, all-α-helical GLTP-fold dictate SL polar headgroup selectivity via differing sequence motifs (DxxxK…RxxxRxxR…H in CPTPs; DxxxNxxK…WxxR…H in GLTPs) but conserved 3D topology to form surface-localized SL headgroup recognition centers, which connect to an internal hydrophobic pocket that accommodates the SL hydrocarbon chains. The targeting of the ceramide moiety originates from the highly conserved spatial locations of Asp and His in the SL recognition center that bind in pincher-like fashion with the ceramide amide group (1–12).

Mechanistically, small single-domain GLTP super-family members, such as CPTP and GLTP, function as 'soluble shuttles' that transit between membranes to acquire and deliver their lipid cargo (4, 5, 13, 14). The only known exception is for the much larger multi-domain FAPP2, which uses a N-terminal pleckstrin homology (PH) domain to target and dock with membranes containing phosphatidylinositol 4-phosphate whereas its C-terminal glycolipid-binding

*For correspondence: Rhoderick E. Brown, reb@umn.edu; Yong-Guang Gao, gaoxx110@umn.edu.

GLTP domain transits back and forth to transfer glycosphingolipids to nearby destination membranes (9, 12, 15–17). As such, FAPP2 can be classified as an LTP anchored at membrane contact sites. In this regard, FAPP2 is similar to the non-GLTP superfamily member, ceramide transfer protein (624 a.a.). Like FAPP2, ceramide transfer protein relies an N-terminal PH domain to target phosphatidylinositol 4-phosphate and help guide interaction with specific membranes but uses a C-terminal StAR-related lipid transfer domain to bind ceramide during the back and forth shuttling needed to redistribute ceramides between closely apposed membranes (18, 19). So, although the issue of what guides FAPP2 to specific membranes is reasonably well established, only recently have insights begun to emerge for small, single-domain GLTP superfamily members. CPTP has been shown to harbor-specific sequence motifs within its membrane interaction region that interact with select cytoplasm-facing anionic phosphoglycerides (e.g., phosphatidylserine and specific phosphoinositides) to enhance operating efficiency by optimizing protein orientation during membrane docking (20, 21).

Insights into the in vivo functional and pathophysiological roles of GLTP superfamily members also have recently begun to emerge (10, 11, 14, 22, 23). The advances implicate human GLTP superfamily member expression in the regulation of the following: *i*) cell-cycle arrest and necroptosis induction in certain colon cancer cell lines (23); *ii*) neuronal myelination and Niemann-Pick type-C disease (24); *iii*) hepatitis C viral infectivity (25); *iv*) cytoplasmic phospholipase A2α activation associated with pro-inflammatory eicosanoid production (10); *v*) autophagy induction and inflammasome assembly that drive surveillance cell release of interleukin-1β and interleukin-18 inflammatory cytokines (22). Owing to the emerging roles of ClP-transferring GLTP superfamily members in pathophysiological situations involving inflammation and autophagy, a need exists to better understand the functional dynamics that enable membrane interaction, SL uptake/release, and the atypical-bound lipid orientation associated with the GLTP protein superfamily. Herein, we report insights gained into the associated dynamic conformational features of human CPTP using molecular dynamics (MD) simulations.

MATERIALS AND METHODS

Preparation of membrane-embedded CPTP

CPTP orientation and position in the membrane was initially estimated using the Orientation of Proteins in Membranes (OPM) program (26–28). The protein was then embedded into a lipid bilayer using the Chemistry at HARvard Macromolecular Mechanics (CHARMM)-GUI membrane builder (29–32). Both the outer and inner membrane leaflets were composed predominantly of POPC but sometimes contained ClP (2.5 mol%) and/or phosphatidylinositol 4,5 bisphosphate (PI-(4,5)P₂) (10 mol%). The membrane/protein system was fully solvated with TIP3P water (33) and buffered in 150 mM NaCl to keep the system neutral. The resulting system (~39,500 atoms) that included 93 POPC molecules was contained in a $60 \times 60 \times 120$ Å³ simulation box. CPTP embedding in one side of the bilayer resulted in the opposite bilayer side without protein having 53 POPC molecules with average surface areas of ~68.6 Å²/molecule. This value mimics the lipid packing in fluid-phase phosphatidylcholine (PC) bilayer vesicles determined by X-ray and neutron diffraction studies (34, 35).

Molecular dynamics simulations

MD simulations were carried out with NAMD2.9 (36) using CHARMM36m (37) parameters set to model the system. NAMD is a parallel, object-oriented molecular dynamics code designed for high-performance simulation of large biomolecular systems and is CHARMM file-compatible. CHARMM3m provides improved accuracy in generating force fields for proteins polypeptide backbone conformational ensembles (37) and is compatible with CHARMM-GUI 6 force fields that enable interactive building of all-atom protein/membrane or membrane-only systems for MD simulation through an automated optimized process. The fast Fourier transform grid information of the Particle-mesh Ewald method is generated automatically. Particle-mesh Ewald method has become a standard method for treating long-range electrostatics in molecular simulations and is widely used because of its high efficiency, which stems from the use of fast Fourier transforms. Simulation systems were subjected to Langevin dynamics and the Nosé-Hoover Langevin piston method (38, 39) to maintain constant pressure (1.01325 Pa = 1 atm) and temperature (T = 303.15 K) (NPT ensemble). The simulations were first optimized by the standard CHARMM-GUI 6-step equilibration and minimization, as illustrated in supplemental Fig. S1, before initiating 300-ns unrestrained production simulations. Visual molecular dynamics software was used to display, analyze, and animate trajectories (40).

Clustering analysis

For the 300 ns trajectory of the protein/membrane system, the clustering was carried out using TTClust (41). Ten classes were obtained, and a representative conformation from each class was generated automatically for subsequent analysis.

Analysis of protein ligand interaction

The protein-ligand interaction profiler Server (42) was used to analyze the interaction between protein and its ligands. The Visual molecular dynamics tool ContactFreq.tcl was used to calculate the contact between ligand and protein residues from the MD simulations with contact being defined as <4 Å distance.

RESULTS

Current insights into the topology of CPTP membrane interaction are based almost entirely on comparisons with GLTP because GLTP has been more

comprehensively characterized, and both proteins share the all α-helical GLTP-fold as their fundamental structural platform (1–10). In the case of GLTP, functional mutation analyses and topology modeling using the OPM and Positions of Proteins in Membranes (PPM) programs have yielded insights into the protein's spatial orientation and positioning during interaction with the lipid bilayer (4, 6, 10, 43–50). In CPTP, the same general surface region has been implicated in membrane interaction as that of GLTP, but other details remain unclear (5, 10).

CPTP membrane interaction during MD simulation

OPM/PPM modeling relies on an implicit solvation model for the lipid bilayer to approximate protein positioning and calculate membrane penetration (26–28) but does not provide insights into the dynamic changes experienced by CPTP during membrane-lipid interaction or lipid-cargo binding. Thus, we applied MD simulations to CPTP and analyzed four states associated with the protein's intermembrane transfer function of ClP. The four CPTP states involve shuttling of either the apo- or holo-forms through the aqueous phase between membrane-lipid bilayers and interaction of either the apo- or holo-forms with membrane-lipid bilayers to achieve ClP uptake or release (supplemental Fig. S2). These states reflect mechanistic stages obtained for GLTP by kinetic, thermodynamic,

and equilibrium binding analyses (43, 50) as well as X-ray crystallography (1–8).

Before initiation of the 300 ns MD simulations, the starting conditions for protein orientation and penetration depth into the POPC bilayer were set up using OPM/PPM modeling and then were optimized by the standard CHARMM-GUI 6-step equilibration and minimization. **Figure 1**A provides a resulting snapshot of CPTP with bound ClP interacting with the POPC bilayer. Tracking of the position of CPTP's center of mass with respect to the POPC bilayer mid-plane indicated that the protein's shallow penetration depth into the POPC bilayer remains nearly unchanged throughout the 300 ns MD simulation (Fig. 1B). Monitoring of the root-mean-square deviation(RMSD) values of the protein backbone atoms revealed somewhat similar profiles (Fig. 1C) for each of the four CPTP states associated with membrane interaction and ClP uptake/release (supplemental Fig. S2). Root mean square deviation values increased slightly (1.0–1.5 Å) over the initial 60 ns but then exhibited mostly small fluctuations ($\leq$0.5 Å) for the remaining 240 ns, thus validating the stability of each protein state. Neither ClP binding to CPTP nor CPTP interaction with the POPC bilayer in the apo- or holo-forms triggered major changes in the overall dynamics and stability of CPTP.

We next identified CPTP residues that most frequently maintained contact with the POPC bilayer
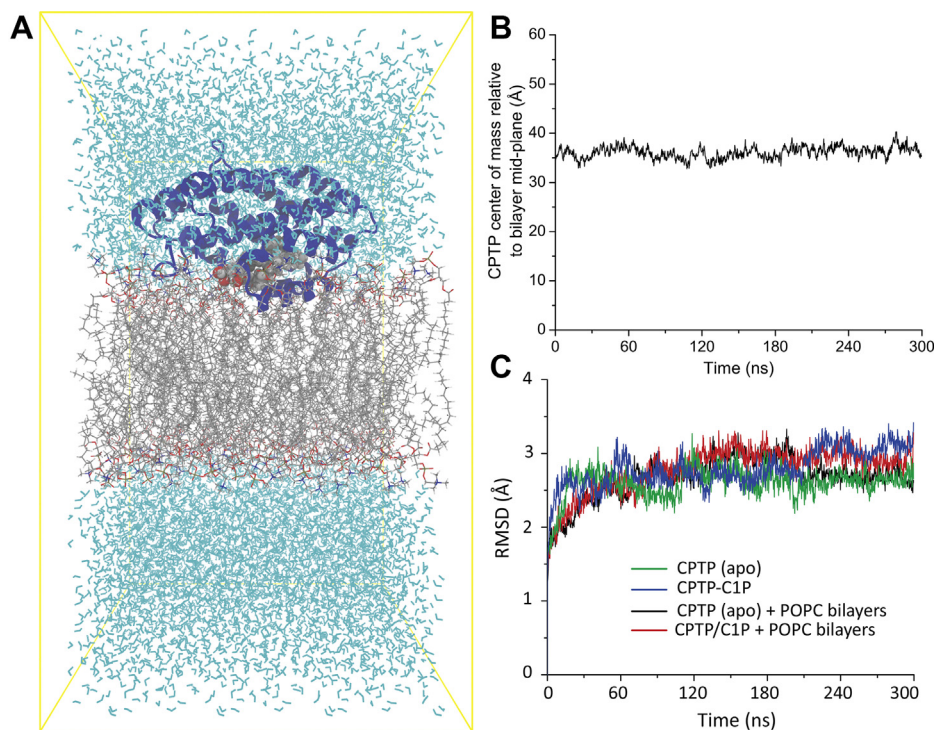

Fig. 1. MD simulation of CPTP. A: The initial configuration for the simulation of the system. The protein is represented in its secondary structure (dark blue). ClP (space-filling) and POPC (stick) hydrocarbon chains are gray with oxygens colored red; nitrogen, blue; and phosphate, orange. The water molecules are cyan. The whole system is boxed with yellow lines. B: CPTP center of mass location relative to POPC bilayer mid-plane versus simulation time. *Y*-axis value of 0 Å = bilayer mid-plane and value of ~20.5 Å = phosphate in POPC headgroup. C: Root-mean-square deviations (RMSD) of CPTP backbone versus simulation time for each CPTP state shown in supplemental Fig. S2.

during the 300 ns MD simulation. Table 1 shows the residues of the CPTP–ClP complex with membrane contact frequencies of 40% or higher. Notably, these residues reside mostly in α-helix 6 and in the N-terminal end of α-helix 2, are located on the external surface of CPTP, and are known to interact favorably with lipid bilayers. **Figure 2**A–D illustrate the positioning of many of the involved residues in relation to the POPC bilayer.

To obtain additional insights into how the local dynamics of various CPTP structural elements are affected by ClP binding to CPTP in the presence or absence of the POPC bilayer, we analyzed CPTP residue dynamics as a function of sequence (**Fig. 3**A). Perhaps not surprisingly, residues forming the connecting loops that link various helices tended to show increased dynamics compared with residues forming the α-helices. It is noteworthy that residues of the α-3/α-4 helices connecting loop exhibited exceptionally high overall dynamics that were clearly impacted by the presence or absence of the POPC bilayer and by the presence or absence of bound ClP. It also is noteworthy that the simultaneous presence of bound ClP and the POPC membrane increased the α-2 helix amino-end dynamics in CPTP but decreased the dynamics of the α-3/α-4 helices connecting loop and the COOH-terminal region residues. In apo-CPTP, in the absence of the POPC bilayer, relatively high dynamics were observed for not only the residues of the α-3/α-4 helices connecting loop, but also for residues of the α-4/α-5 helices connecting loop and many of those comprising the α-6 helix, the adjacent α-6/α-7 connecting loop, and the COOH-terminal region.

TABLE 1. POPC bilayer membrane contact frequencies of CPTP residues

Residue[a]	Location[b]	Contact Frequency[c]
PHE-52	α2-helix	87.86
ILE-49	α2-helix	73.45
LYS-55	α2-helix	69.78
ILE-53	α2-helix	61.04
ASP-56	α2-helix	51.23
THR-48	α2-helix	47.70
SER-51	α2-helix	46.56
ALA-157	α6-helix	76.05
VAL-160	α6-helix	69.11
VAL-153	α6-helix	67.71
VAL-154	α6-helix	65.98
ARG-156	α6-helix	60.37
THR-164	α6-helix	59.24
CYS-163	α6-helix	56.77
PRO-151	α6-helix	56.37
TRP-152	α6-helix	54.17
THR-159	α6-helix	41.09
SER-135	α5-helix	44.03
GLY-47	α1-α2 loop	61.51
ARG-133	α4-α5 loop	52.30
LEU-165	α6-α7 loop	43.76

[a]Data is for CPTP–Cl6-ClP complex.
[b]Location = CPTP PDB: 4k84.
[c]Values = % time interacting with POPC bilayer; CPTP residues listed have contact values >40%.

The α-3/α-4 helices connecting loop in the GLTP-fold has previously been implicated in the regulation of the differing glycolipid specificity in FAPP2-GLTPH domain and GLTP (12), and more recently has been found to harbor a PI-(4,5)P_2 docking site in CPTP (21). Therefore, we analyzed the dynamics associated with the α-3/α-4 helices connecting loop in more detail. To do so, we partitioned the 1,500 total frames generated during the 300 ns MD simulation into 10 clusters using TTClust (41). TTClust helps ascertain which differences are only fluctuations of the system versus which are linked to different conformations. Figure 3B, C illustrate differing conformations that the α-3/α-4 helices connecting loop can assume when CPTP-containing bound ClP interacts with the POPC bilayer, as revealed by TTClust, relative to the X-ray crystallographic structure of the holo-protein determined in the absence of the POPC bilayer. The dynamic flexibility of the α-3/α-4 helices connecting loop enables close approach to the phosphoglyceride headgroup region of the bilayer (supplemental Video S1), consistent with recent findings indicating the presence of a PI-(4,5)P_2 docking site within the α-3/α-4 helices connecting loop (21).

Dynamics associated with bound ClP in CPTP

We also investigated the dynamics of 16:0-ClP when bound within the ClP-specific hydrophobic pocket of the protein. The 16:0-ClP polar headgroup was found to remain relatively flexible when interacting with the sphingolipid headgroup recognition site located near the protein surface (Fig. 3D). In contrast, the 16:0-ClP hydrocarbon chains remain relatively rigid and constrained when enveloped within the hydrophobic pocket consistent with a 'tight fit' within a minimally expanded pocket. Altogether, ClP remained within the confines of the pocket but displayed limited, dynamic back-and-forth sliding action along the pocket's long axis. It is noteworthy that the 16:0-ClP orientation within the SL binding pocket of CPTP, that is, hydrocarbon chains inserted deeper than the polar headgroup, is opposite that of various other LTPs (13, 14, 46–50) in which the lipid polar headgroup is buried deeper than the hydrocarbon chains.

Changes in CPTP dynamics induced by changes in bilayer lipid composition

To gain insights into apo-CPTP interaction with bilayers composed of differing lipid compositions. MD simulations were performed using the following: *i*) 100% POPC; *ii*) POPC containing Cl6-ClP; *iii*) POPC containing PI-(4,5)P_2; and *iv*) POPC containing both Cl6-ClP and PI-(4,5)P_2 (Fig. 3E). When present, Cl6-ClP became bound within the SL binding site of CPTP during the 300 ns simulation. The low Cl6-ClP bilayer concentration (2.5 mol%) was used to mimic the physiological situation of ClP being transported by CPTP soon after synthesis by ceramide kinase located in the
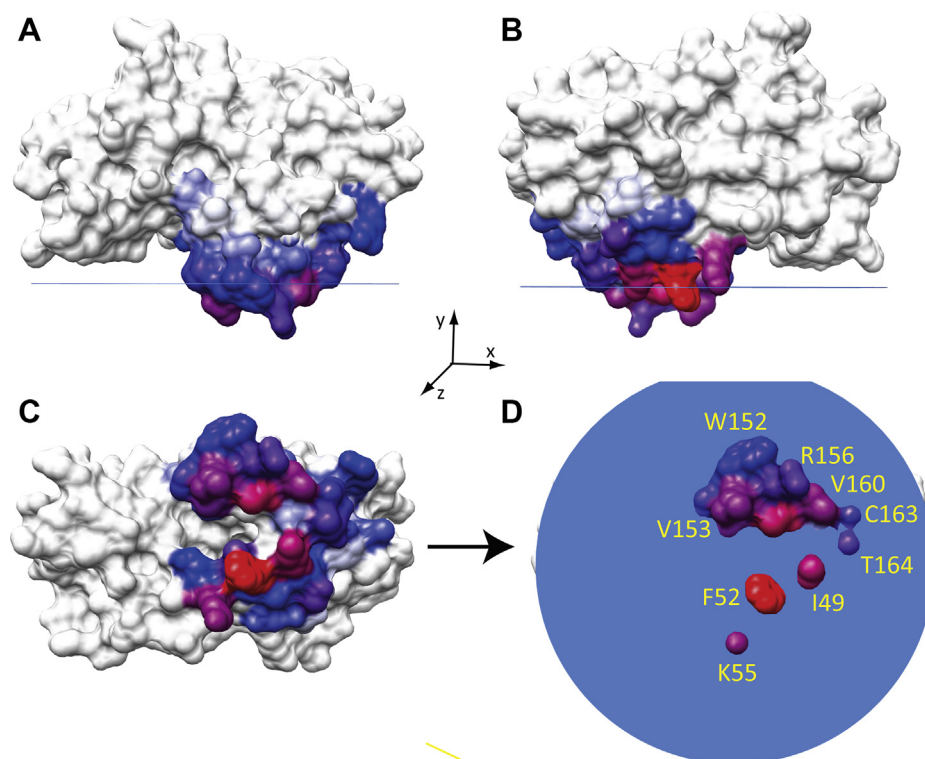
Fig. 2. CPTP orientation during contact with a POPC membrane interface. A: CPTP (space-filling); (B) CPTP (space-filling); view = 180° rotation in the *y*-axis relative to (A). C: CPTP (space-filling); view = 90° rotation in the *x*-axis relative to (A). D: CPTP (space-filling); same view as (C) but with membrane polar/nonpolar interface (blue circle) as shown. The blue-to-red colors in CPTP correspond to membrane contact frequencies over the range of 54–88% (Table 1).

trans-Golgi. The data show that the largest increases in the RMSF values for CPTP residues were observed for the α-3/α-4 helices connecting loop when the POPC bilayer contained both ClP and PI-(4,5)P$_2$ (Fig. 3E ,blue trace). This finding is consistent with a recent study showing CPTP transfer activity stimulation via a PI-(4,5)P$_2$ headgroup interaction site containing a di-Arg motif in the α-3/α-4 helices connecting loop (21).

Lipid rearrangement induced by α-helix 6 of CPTP

We next investigated the impact of CPTP on the dynamic conformational states of nearby POPC molecules within the lipid-bilayer matrix. Notably, α-helix 6 was found to be unique in its ability to strongly affect POPC dynamic conformations, with respect to the lipid's orientation within the bilayer. As illustrated in **Fig. 4**, the POPC hydrocarbon chains were found to partially 'wrap' around the α-helix 6 membrane-facing exterior surface, whereas R156 interacted with the POPC phosphate and acyl-amide polar groups (Fig. 4D). This observation led us to hypothesize that the bilayer normal positioning of α-helix 6 combined with its preponderance of nonpolar residues and other residues (e.g., Arg and/or Lys) that are able to favorably interact with phosphoglyceride amphiphiles promote the large conformational changes observed in the interacting POPC hydrocarbon chains. We further hypothesized that the ability of the α-6 helix exterior surface to

induce repositioning and partial 'wrapping' of the POPC hydrocarbon chains could reflect a mechanism used to orient and guide ClP to and from the nearby ClP-selective binding pocket. To gain further insights, we first examined X-ray crystallographic diffraction data showing the different ways that ClP can interact with the plant CPTP homolog, ACD11 (PDB: 4NTI) (11). In ACD11/ClP, cocrystallization of protein and sphingolipid reveals ClP interacting with α-6 helix as well as occupying the ClP-specific binding/transfer site (**Fig. 5**A). Close examination of the α-6 helix interactions with ClP shows R148-K149 di-cationic site involvement that includes formation of a salt bridge by K149 with the ClP-phosphate group and hydrogen bonding by the K149 side chain with the carbonyl oxygen of the amide linkage in a second ClP molecule (Fig. 5B). Also evident is the R148 hydrogen bonding with the phosphate group of a ClP molecule, whereas its hydrocarbon chains undergo van der Waals contacts with the indole ring of W145 in ACD11 (Fig. 5C).

Because of the existence of the structurally analogous R155-R156 di-cationic site in CPTP (12), we used MD simulations to test whether the ACD11 crystallographic findings might reflect a role for α-helix 6 R156 in the uptake of ClP. To do so, we initially generated a model of a POPC bilayer containing one ClP molecule positioned such that the ClP headgroup was near the α-6 helix di-Arg group of apo-CPTP. The orientation
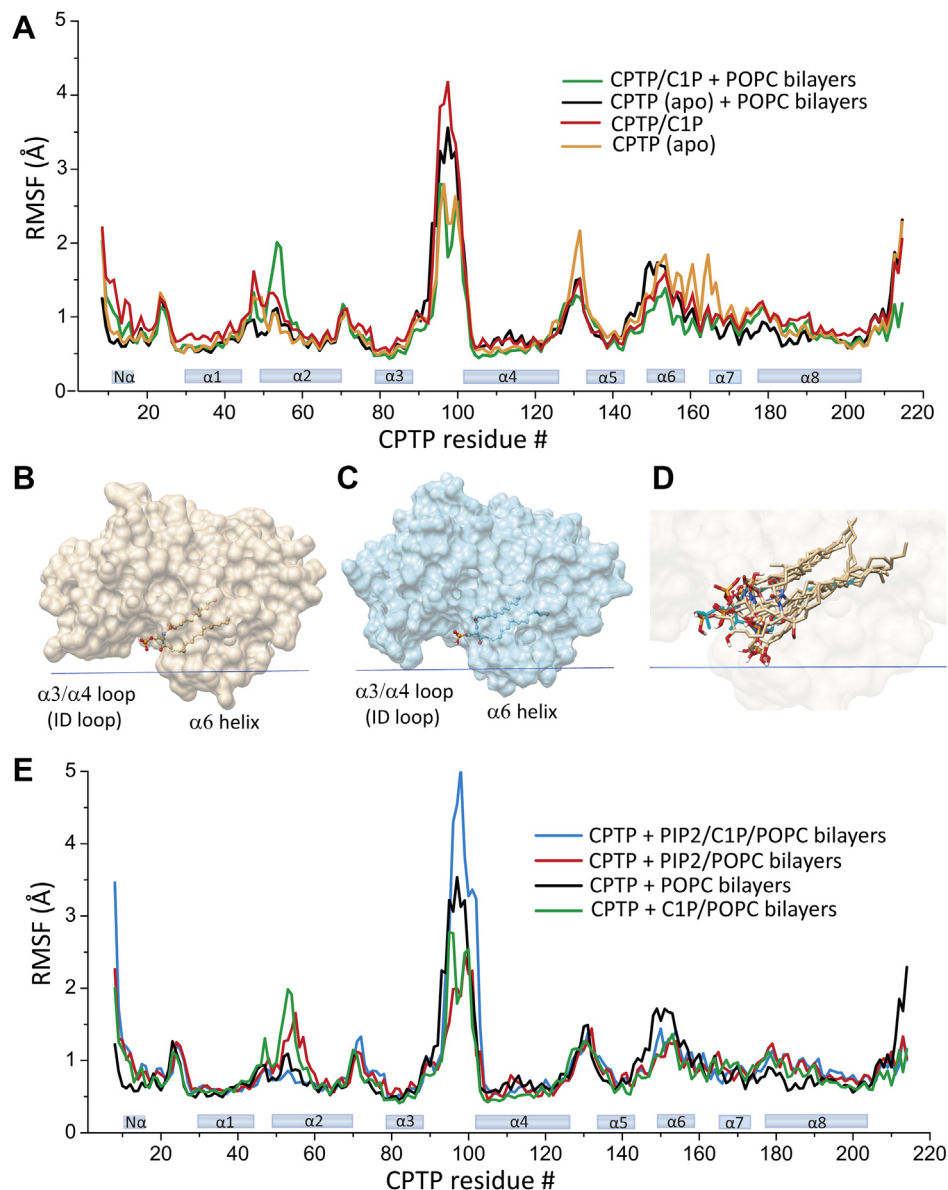
Fig. 3. Dynamics of CPTP residues and C1P detected by MD simulation. A: RMSF plot of CPTP residues by sequence from the trajectories of 300 ns. Four different states associated with CPTP transfer of C1P are compared. B: Space-filling representation of CPTP/C1P crystal structure (PDB: 4k84). C: Snapshot of the CPTP–C1P complex from a cluster of the MD simulations indicates flexibility of α3/α4 helices connecting loop (ID loop) that enables close approach to the membrane lipid polar headgroups. D: Ten representative structures of C1P from 10 simulation clusters superpositioned to show the dynamics of C1P during simulation. C1P with cyan hydrocarbon chains is from the crystal structure (PDB: 4k84). E: RMSF plot of CPTP residues by sequence from 300 ns trajectories showing apo-CPTP interacting with bilayers composed of 100% POPC or POPC containing either C16-C1P or PI-(4,5)P$_2$ or POPC containing both C16-C1P and PI-(4,5)P$_2$.

and penetration depth of the apo-CPTP into the lipid bilayer relied on OPM/PPM modeling followed by placement of the CPTP/C1P/POPC membrane system in a water box using the Charmm-GUI server. MD simulations were then performed for 20 ns on the final system to determine if the dynamic C16-C1P conformation is affected by CPTP in similar ways as observed for POPC. **Figure 6** shows that C1P did transition to a more membrane-interface-parallel orientation with its hydrocarbon chains interacting with the membrane-exposed surface of α-6 helix in CPTP (supplemental Video S2). The contact frequencies of various residues

in CPTP α-6 helix with C16-C1P during first 20 ns of the MD simulation are summarized in Table 2. Interestingly, the high contact frequencies for Trp152 and Arg156 in the simulation model correspond well with the crystallographic close contacts observed with analogous, similarly positioned residues in plant CPTP ACD11. Note that when C16-C1P in the POPC membrane was replaced by C1P with a short hexanoyl acyl chain (6:0), the C6-C1P phosphate headgroup remained poorly engaged with α-6 helix (that contains the R155-R156 di-Arg motif) and failed to wrap beneath α-6 helix during the initial 20 ns of the MD simulation
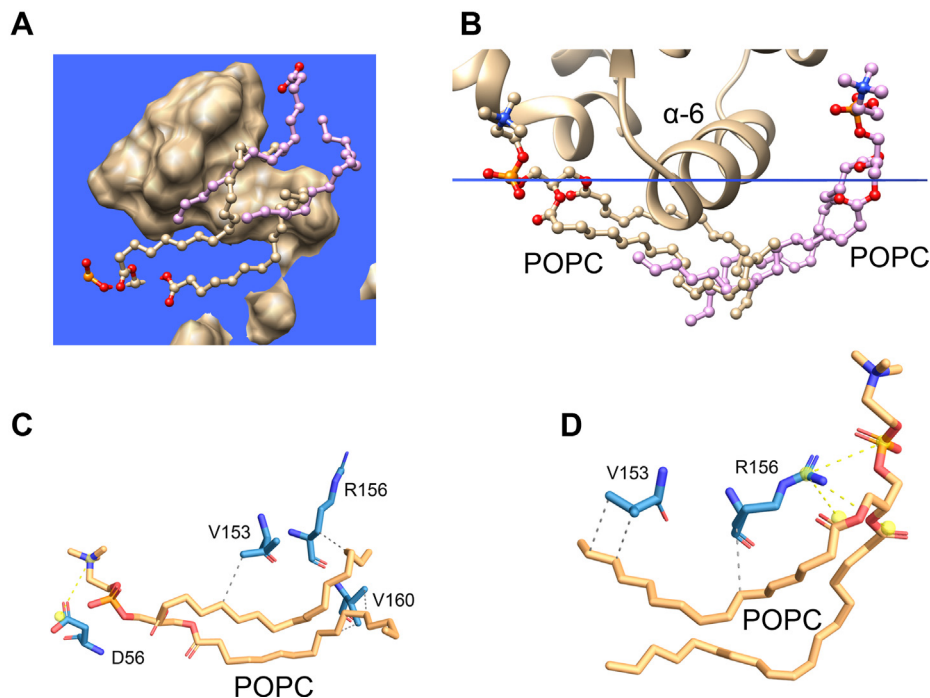
Fig. 4. POPC rearrangement induced by CPTP α-6 helix detected by MD simulation. A: Membrane-penetrating region of CPTP (beige space-filling) viewed from inside the membrane looking toward the hydrocarbon/POPC polar headgroup interface (blue square). The POPC hydrophobic acyl chains (ball & stick format) become horizontally aligned with the membrane interface and 'tunnel' beneath the under-surface of CPTP by interacting with α-6 helix. B: Zoom view of α-6 helix region from end-on perspective. C: 3D map of interactions between CPTP α-6 helix residues (V153, R156, V160, and D56) and a POPC. D: 3D map of interactions between CPTP α-6 helix residues (V153 and R156) and a POPC.

(supplemental Video S3), a finding that could reflect competition by the more abundant POPC, which also can interact with R156 and has two long acyl chains that can wrap around the membrane-facing external surface of α-6 helix.

DISCUSSION

The human branch of the GLTP superfamily consists of four members: GLTP, FAPP2, CPTP, and GLTPD2 (14). Orthologs of GLTP, FAPP2, and CPTP have also been identified in many other eukaryotes and characterized in filamentous fungi and plants (5, 11, 12, 14, 51–57). From the structural perspective, the most extensively characterized superfamily members are human GLTP and CPTP, and the plant CPTP ortholog, ACD11, which account for 37 X-ray crystallographic deposits (90%) in the Protein Data Bank. The MD simulations presented here provide the first insights into the conformational dynamics of CPTP transition states linked to the sphingolipid transfer process such as CPTP interaction with the membrane bilayer and the binding of the C1P cargo sphingolipid by CPTP. No such insights have existed previously for any GLTP superfamily member.

The challenges associated with various modeling options involving membrane interaction by lipid transfer proteins and other peripheral membrane proteins have recently been reviewed by (58). Extensive

efforts for the lipid parameterization set have led to widespread use of CHARMM36, which can be applied without the need for an external surface tension while faithfully reproducing the physicochemical properties of a wide variety of lipid bilayers (59, 60). Our choice for using POPC for initial MD simulation studies of CPTP conformational dynamics associated with fluid-phase bilayer matrix interaction reflects this PC species often being a major biomembrane component as well as having an asymmetric acyl composition with the sn-1 chain being long and saturated (C $\geq$ 16) and the long sn-2 chain (C $\geq$ 18) containing cis unsaturation. Such an acyl chain arrangement has interesting biological consequences including more efficient membrane vesiculation and lower membrane permeability compared with phosphoglycerides containing two saturated or polyunsaturated chains (61). As mentioned in the Materials and methods, we performed our MD simulations using POPC at average surface areas of ~68.6 Å^2/molecule as a means to mimic the lipid packing in planar fluid-phase PC membranes with sn-2 monounsaturated acyl chains. Future MD simulation studies will be needed to address the effect of changes in average POPC surface area/molecule on CPTP interaction as associated with curvature-stressed outer surfaces present in small lipid bilayer vesicles often used for protein-mediated lipid intervesicular transfer measurements due to their high response sensitivity, that is, faster lipid transfer rates. It is noteworthy that
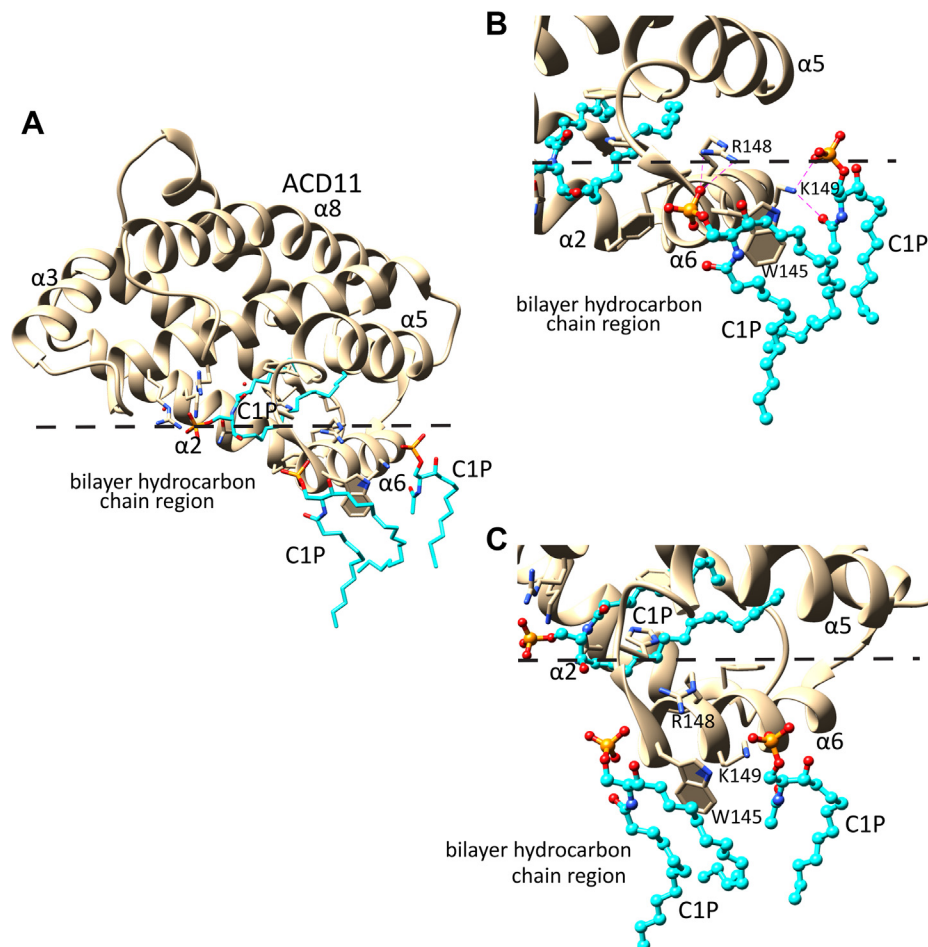
Fig. 5. ClP interaction with α-6 helix detected by X-ray crystallography of ACD11/ClP. Two ClP interaction sites are evident on α-6 helix other than ClP occupying the hydrophobic binding pocket of CPTP. The dashed lines indicate the position of the polar-to-nonpolar interface as defined by the acyl ester linkages of POPC. ClP molecules interacting with the α-6 helix and the hydrophobic binding pocket are depicted with cyan hydrocarbon chains, red oxygens, blue nitrogens, and orange phosphates. A: Structure of ACD11/ClP (PDB: 4NTI). B, C: Zoom views from end-on and parallel perspectives of α-6 helix showing the positioning of ClP-interacting residues R148, K149, and W152.

previous lipid monolayer studies involving GLTP (44, 45, 62, 63) have shown that surface pressure changes (that alter the average surface area/lipid molecule) do affect the GLTP-mediated glycolipid transfer rate and GLTP penetration into lipid monolayers composed of various phosphoglycerides. Yet, the air/water interface of lipid monolayers present a different environment for the lipid-acyl chains than that of the bilayer mid-plane, complicating direct comparisons between POPC monolayers versus POPC bilayers based on lipid packing. In any case, we expect that future MD simulations will provide bilayer data that will be qualitatively supported by the earlier lipid monolayer findings for GLTP, while also providing insights into the CPTP regions most impacted with respect to their conformational dynamics.

MD simulations of other lipid binding/transfer proteins include studies of various fatty acid binding proteins, plant nonspecific lipid transfer proteins, and phosphatidylinositol transfer protein (64–71). The

fundamentally different structural organizations of the preceding proteins, sometimes including stabilizing internal disulfides, prevent meaningful insights from being gained into the conformational dynamics associated by comparisons with the structurally unique all-α-helical GLTP-fold of CPTP. In the GLTP-fold, intramolecular conformational stability and dynamics are maintained and regulated by cation-π and π-π stacking interactions, van der Waals contacts, and salt bridges, but not by disulfide bridging (1, 9, 12, 54). Accordingly, thermally-induced denaturing profiles for GLTP superfamily members such as GLTP indicate rather low unfolding temperatures (≤55°C) (5, 9, 72).

Our MD simulations took advantage of existing X-ray crystallographic data that define CPTP global conformation and of OPM/PPM modeling for initial protein positioning and orientation for membrane interaction. Not surprisingly, internally oriented residue side-chains directly involved in CPTP forming its GLTP-fold tend to exhibit less flexibility than residue
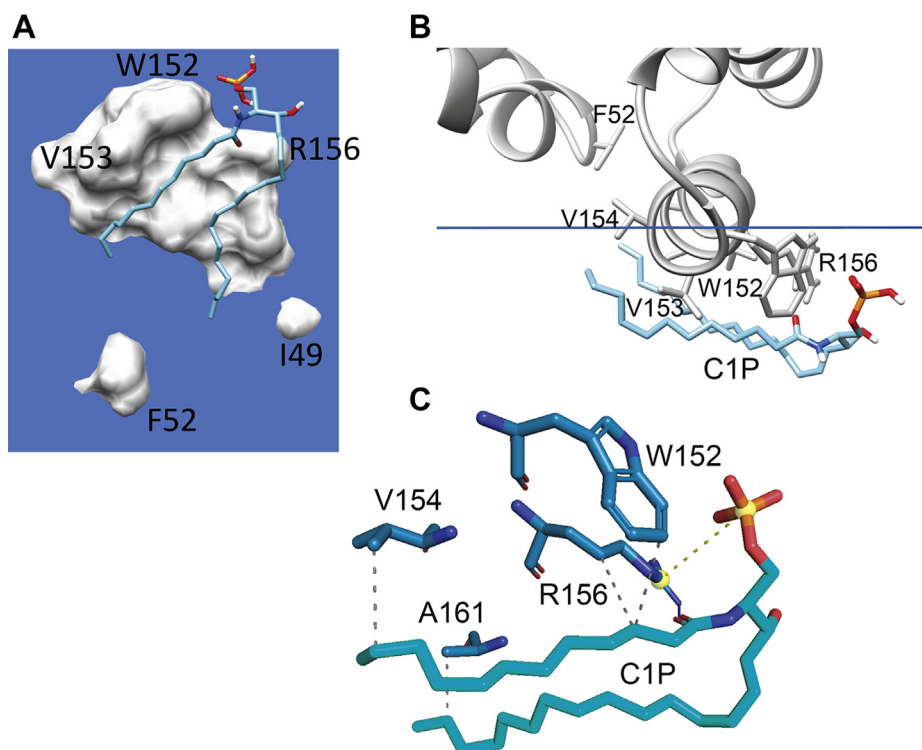
Fig. 6. Cl6-ClP rearrangement induced by CPTP α-6 helix during MD simulation (e.g., supplemental Video S2). Cl6-ClP is shown in stick representation with cyan hydrocarbon chains, red oxygen, blue nitrogen, and orange phosphate. A: View from beneath the bilayer interface (blue). CPTP residues are shown as space-filling. B: End-on view of α-6 helix aligned with the bilayer interface (blue line) showing the repositioning of ClP induced by interacting α-6 helix residues R156, W152, V153, and V154. C: Zoom view of ClP interacting with α-6 helix residues W152, R156, V154, and A161.

side-chains residing on the CPTP outer surface. In addition, CPTP regions consisting of α-helices are generally less dynamic than loops linking the α-helices together. No large scale conformational changes associated with 'transition' states/stages directly related to CPTP function are evident in the dynamics exhibited by apo-CPTP and holo-CPTP in the absence and presence of the POPC bilayer. Yet, it is noteworthy that residues of the α-3/α-4 helices connecting loop collectively exhibit relatively high overall dynamics that clearly are impacted by the presence or absence of the POPC bilayer and by the presence or absence of bound ClP. Other CPTP regions measurably but less so affected by similar conditions include increased dynamics by α-helix 2 amino-end residues but decreased

TABLE 2. CPTP α-helix 6 residue initial contact frequency with Cl6-ClP in POPC bilayer

α6-Helix Residue[a]	Contact Frequency[b]
TRP-152	99%
VAL-153	55%
VAL-154	3%
ARG-156	97%
ALA-157	58%
VAL-160	24%
ALA-161	4%

[a]α-6-helix of CPTP.
[b]Values = % interaction time with Cl6-ClP versus POPC during first 20 ns of simulation.

dynamics by the α-3/α-4 helices connecting loop and the COOH-terminal region residues. The findings are consistent with these protein regions being located in close proximity to the membrane bilayer interface and near the sphingolipid recognition center where they likely play a role in ClP acquisition/release during the SL intermembrane-transfer process. The finding of the α-3/α-4 helices connecting loop dynamically approaching the membrane surface is noteworthy because recent studies have implicated this loop in harboring a PI-(4,5)P$_2$ docking site that enhances the ClP transfer activity of CPTP (21) and regulating the differing glycolipid specificity in FAPP2-GLTPH domain and GLTP (12).

The MD simulations here indicate that α-helix 6 of CPTP is the dominant structural element driving membrane bilayer interaction, a finding supported by earlier mutation and OPM/PPM modeling studies of the GLTP-fold of human GLTP (1, 4, 5, 10, 20, 22, 43–49). Indeed, GLTP interaction with the POPC bilayer has previously been found to be relatively nonperturbing, as expected for shallow penetration by α-6 helix that is limited to one side of the bilayer (43). The MD simulations also support the overall position and orientation of CPTP remaining relatively stable during interaction with the POPC bilayer, although penetration depths for α-helix 6 fluctuate modestly with respect to the average location of surrounding lipid-bilayer interface. Our

data enable estimation of penetration depths by CPTP structural elements that directly interact with the POPC bilayer, that is α-helix 6, the N-terminal region of α-2 helix, α-3/α-4 helices connecting loop. To do so, we initially considered structural parameters determined for liquid-crystalline (Lα phase) bilayers consisting of di-oleoyl PC (35, 73). Such parameters include the distances of choline (21.87 Å), phosphate (20.17 Å), and the acyl chain carbonyl groups (15.98 Å) from the bilayer mid-plane as well as phosphorylcholine headgroup parameters such as orientation (22 ± 4°) respect to the bilayer interface and the nitrogen-to-phosphate distance (4.5 Å). Using the acyl carbonyl groups as markers of the headgroup/hydrocarbon boundary (26–28), the polar headgroup region thickness equals ~8.5–9.0 Å (based on ~5.9 Å for the acyl carbonyl group-to-choline nitrogen distance allowing plus 2.5–3.0 Å for hydration of choline). Notably, in the CPTP/POPC membrane, MD simulation yields average distances of 21.3 Å for choline-to-bilayer mid-plane and 20.1 Å for phosphate-to-bilayer mid-plane, values that agree well with the data obtained by X-ray and neutron diffraction (35, 73). Based on this agreement, we estimated the MD simulation distances from the bilayer mid-plane to the α-helix 6 Trp152 and Arg156 side-chains to be 14.6 (±1.3) and 15.3 (±1.0) Å, respectively. Table 3 summarizes this data as well as distances calculated for residues in the N-terminal region of α-helix 2 (e.g., Ile49, Phe52, Ile53, and Lys55) that embed in the POPC bilayer and residues of the α-3/α-4 helices connecting loop (R^{90}LVDLERRSHHPE^{102}) that dynamically approach the POPC headgroups of the bilayer. **Figure 7** provides a summary schematic (drawn to scale) of CPTP interacting with one half of a POPC bilayer.

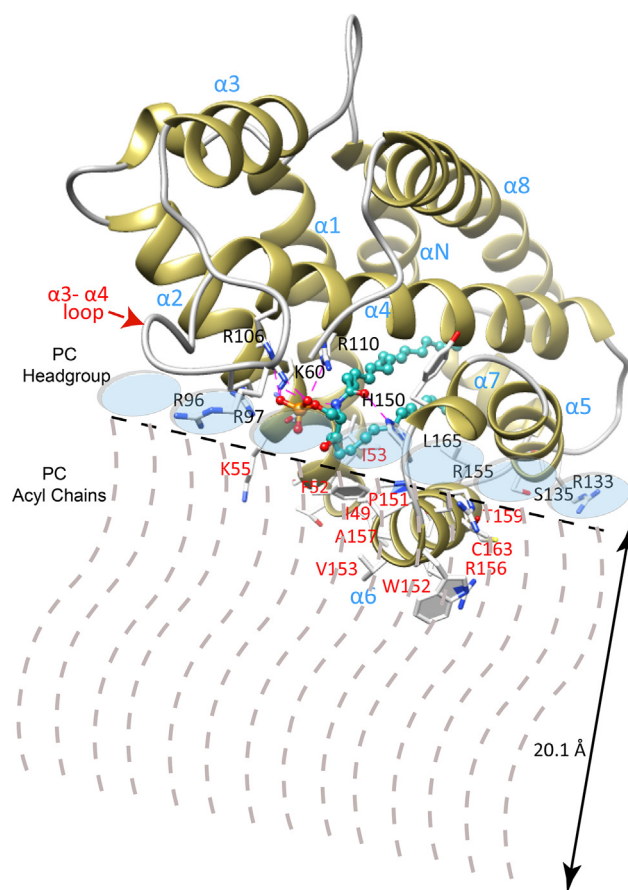Notably, the MD simulations indicate that α-6 helix does more than function as a simple membrane

Fig. 7. Scale model of CPTP orientation and penetration depth into POPC bilayer leaflet revealed by MD simulations. CPTP interaction is dominated by α-6 helix and the N-terminal region of α-2 helix. Residues that penetrate into the upper hydrocarbon region are labeled in red. The relatively shallow penetration by the protein supports a model for CPTP scanning the membrane surface to acquire ClP via a lipid-chain reorienting mechanism involving α-6 helix, as illustrated by Fig. 8.

TABLE 3. Model for CPTP/Cl6-ClP penetration depth into POPC bilayer

Residue[a]	Location[b]	Distance from Bilayer Mid-Plane (Å)[c]
TRP-152	α-helix 6	14.6 (±1.3)
VAL-153	α-helix 6	10.4 (±1.4)
VAL-154	α-helix 6	15.1 (±1.1)
ARG-156	α-helix 6	15.3 (±1.0)
ALA-157	α-helix 6	14.5 (±1.0)
VAL-160	α-helix 6	14.3 (±0.9)
PHE-52	α-helix 2	16.5 (±1.6)
ILE-49	α-helix 2	17.7 (±0.9)
LYS-55	α-helix 2	17.2 (±1.3)
ILE-53	α-helix 2	18.2 (±2.0)
GLU-95	α 3/α 4 loop	27.2 (±2.8)
ARG-96	α-3/α-4 loop	22.7 (±2.7)
ARG-97	α-3/α-4 loop	22.6 (±1.8)
SER-98	α-3/α-4 loop	22.3 (±1.9)
HIS-99	α-3/α-4 loop	20.1 (±2.5)
HIS-100	α-3/α-4 loop	24.4 (±2.6)

[a]Data is for CPTP–Cl6-ClP complex.
[b]Location = CPTP (PDB: 4k84).
[c]In POPC bilayer, phosphate distance from bilayer mid-plane ≈20.1 Å (35, 73).

docking element for CPTP. Compared with the other membrane contact regions of CPTP, α-6 helix exerts strong and unique effects on the dynamic conformations of POPC and ClP. When these lipids come into direct contact with α-6 helix via translational diffusion within the bilayer, their hydrocarbon chains transition from bilayer interface normal to bilayer interface aligned orientation. R156 and W152 located near the N-terminal end of α-6 helix are especially important for the reorientation process based on their nearly sustained dynamic contacts with the lipid. The finding for ClP is supported by X-ray crystallography structural data for plant CPTP, ACD-11 (PDB: 4NTI) showing that ClP can interact with the N-terminal end of α-6 helix N-end via K149, R148, and W145 (11). Notably, in control MD-simulations involving CPTP-R156L mutant (supplemental Video S4), the phosphate headgroup of Cl6-ClP did not engage strongly with the mutated α-6 helix, and the Cl6-ClP hydrocarbon chains did not wrap beneath α-6 helix as observed for wild type CPTP. However, this observation should not be construed as

implying that Rl56 is absolutely specific for ClP uptake or essential for CPTP-mediated ClP transfer. Indeed, Rl56 also was observed interacting with the phosphate and acyl-amide groups of POPC (Fig. 4D). Moreover, we know from previous studies of GLTP-fold proteins (including CPTP) that various other α-6 helix residues contribute to the membrane engagement needed for sphingolipid intervesicular transfer to occur. In the case of CPTP, such residues include Trp, Val, Ile, Phe, along with di-Arg (10). In the case of the Rl55/Rl56 di-Arg motif, CPTP-mediated ClP transfer has been partially addressed by Rl55 point mutation (CPTP-Rl55Q) in which slowing, but not complete inhibition, of ClP transfer was observed and decreased CPTP membrane association (21). A more comprehensive study will be needed to further clarify potential 'dual role' of the di-Arg region in the α-6 helix in both CPTP membrane association and ClP transfer. Taken together, these findings lead us to propose that the N-end of α-6 helix functions to reorient and guide ClP to the CPTP binding pocket region. The ClP dynamic behavior that supports our hypothesis for α-6 helix involvement in ClP uptake by CPTP is summarized in **Fig. 8**. Initially, the ClP (A) molecule is aligned with the POPC molecules forming one lamellar surface of the bilayer. Interaction of the ClP phosphate headgroup with the Rl55/Rl56 di-Arg region in α-6 helix serves to help trigger dynamic reorientation that promotes interaction of the ClP nonpolar hydrocarbon chains with α-6 helix Trpl52 and Vall53 via van der Waals contacts, resulting in a horizontal conformation with respect to the bilayer normal (Fig. 8, ClP (B)). The horizontally-reoriented ClP hydrocarbons are more favorably positioned for gaining entry into the ClP-specific binding pocket. This dynamic repositioning, coupled with guidance by Phe52, Ile49, and Ile53 at the N-terminal region of α-2 helix, facilitates ClP hydrocarbon chain 'tunneling' into the ClP binding pocket that is lined with hydrophobic residues (Fig. 8 by ClP (C)). Selectivity for ClP can then occur via the sphingolipid headgroup recognition center interaction with the ClP phosphate and acyl-amide linkage via a conserved Asp^{56}-Lys^{60}∗∗∗∗Arg^{106}-Arg^{110}∗∗∗∗His^{150} three-dimensional motif (5, 10, 12, 14). The final bound ClP position in the CPTP binding pocket is illustrated in Fig. 8 (ClP (D)).

Although the ability of α-6 helix to deform and reorient the hydrocarbon chains of Cl6-ClP is clear, our present data do not reveal whether the ClP acyl chain enters the CPTP hydrophobic pocket before the sphingosine chain. This kind of oriented ClP entry into the CPTP hydrophobic pocket has been implied from X-ray crystallography data that sometimes capture a 'sphingosine-out' ClP binding mode that may play a role in regulating transient homo-dimerization on the membrane surface (5, 6, 10). Future experiments will be needed to address the preceding issue including whether the ClP acyl chain initially undergoes more frequent deformations than the sphingosine chain due
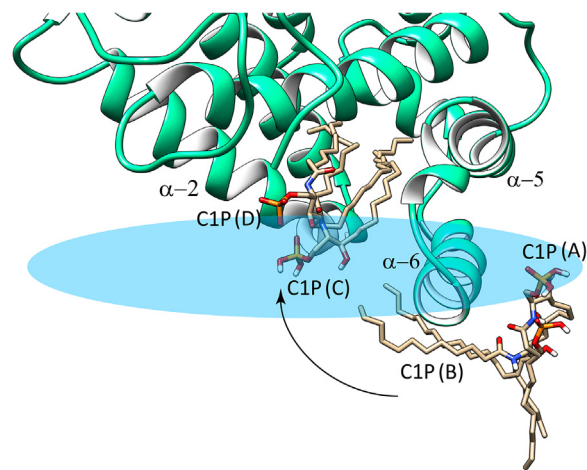

Fig. 8. A model illustrating the functional role of α-6 helix for reorienting and guiding ClP into the binding pocket of CPTP from membrane. The progression of events that lead to ClP binding is shown by four different ClP conformations. ClP (A) represents ClP positioned normally with the POPC bilayer; ClP (B) represents ClP that has become reoriented and repositioned by interaction with α-6 helix where the ClP hydrocarbon chains interact with Trpl52 and Vall53, whereas the ClP phosphate interacts with di-Arg motif (R155 and R156). The reoriented ClP becomes much more aligned with the bilayer interface thus enabling access to the hydrophobic binding pocket of CPTP. ClP (C) is shown sliding into the binding pocket of CPTP. ClP (D) represents ClP secured within the hydrophobic pocket due to the specific interactions of the ClP polar headgroup, that is, phosphate and acyl-amide linkage, with residues that define the ClP recognition motif as previously identified by X-ray crystallography and mutation analyses.

to an oriented ClP interaction with α-6 helix. What currently is clear is that the CPTP binding pocket samples various membrane lipids in sorting-like fashion but can only fully engage with ClP due to the specific ClP recognition interactions. It is interesting to speculate that the dynamic conformational changes to the CPTP α-3/α-4 helices connecting loop that occur when both ClP and PI-(4,5)P_2 are present may be offset or altered when CPTP/ClP encounters a membrane surface containing other 'regulator' phosphoglycerides such as phosphatidylserine or phosphatidic acid to facilitate ClP release (20). Future experiments will be needed to further test this hypothesis.

CONCLUSIONS

The findings gained in the present study from the MD simulations provide the first insights into the conformational dynamics that enables human CPTP to acquire and deliver ClP during interaction with membranes. Penetration by CPTP into the membrane bilayer is confined mostly to α-6 helix and the N-terminal end of α-2 helix, involves only one bilayer leaflet and is relatively shallow. Dynamic, large-scale conformational changes for CPTP during membrane interaction or ClP uptake are minimal except for the α-3/α-4 helices connecting loop which recently was

shown to interact with certain membrane-embedded phosphoinositides. Besides functioning as a shallow membrane-anchoring element, the ability of α-6 helix to deform and reorient membrane lipids is consistent with a proposed functional role in ClP uptake. This finding is noteworthy because the lipid orientations within the binding pockets of various other lipid binding/transfer proteins support a 'polar headgroup first' entry via a different mechanism rather than the 'hydrocarbon chain first' entry that is proposed for the GLTP-fold. It is interesting to note that integral membrane channel proteins that function in the transbilayer migration of specific lipids contain α-helices with similar features that aid in the lipid reorientation needed for successful translocation across the membrane (74–76). Finally, gaining insights into CPTP is important because of this protein's recently revealed role in regulating cytosolic phospholipase A₂α action that drives pro-inflammatory eicosanoid production as well as in autophagy-dependent inflammasome assembly needed for production and release of interleukins (IL-1β and IL-18) by surveillance cells and induction of pyroptosis.

Data availability

All data pertaining to the article and the supporting information are available upon request by contacting Yong-Guang Gao <gaoxx110@umn.edu> or Rhoderick E. Brown <reb@umn.edu>. ▪

Author contributions
Y.-G. G. and R. E. B. conceptualization; Y.-G. G. and J. M. methodology; Y.-G. G. and R. E. B. visualization; Y.-G. G. and R. E. B. writing–original draft; Y. G. G., L. M., D. J. P., and R. E. B. writing–review and editing; Y.-G. G. investigation; Y.-G. G. data curation; Y.-G. G. formal analysis; J. M. resources; R. E. B. supervision; R. E. B. project administration; R. E. B. funding acquisition.

Conflict of interest
The authors declare no competing interests.

REFERENCES

1. Malinina, L., Malakhova, M. L., Teplov, A., Brown, R. E., and Patel, D. J. (2004) Structural basis for glycosphingolipid transfer specificity. *Nature.* **430**, 1048–1053
2. Malinina, L., Malakhova, M. L., Kanack, A. T., Lu, M., Abagyan, R., Brown, R. E., and Patel, D. J. (2006) The liganding of glycolipid transfer protein is controlled by glycolipid acyl structure. *PLoS Biol.* **4**, e362
3. Airenne, T. T., Kidron, H., Nymalm, Y., Nylund, M., West, G., Mattjus, P., and Salminen, T. A. (2006) Structural evidence for adaptive ligand binding of glycolipid transfer protein. *J. Mol. Biol.* **355**, 224–236
4. Brown, R. E., and Mattjus, P. (2007) Glycolipid transfer proteins. *Biochim. Biophys. Acta.* **1771**, 746–760
5. Malinina, L., Simanshu, D. K., Zhai, X., Samygina, V. R., Kamlekar, R., Kenoth, R., Ochoa-Lizarralde, B., Malakhova, M. L., Molotkovsky, J. G., Patel, D. J., and Brown, R. E. (2015) Sphingolipid transfer proteins defined by the GLTP-fold. *Q. Rev. Biophys.* **48**, 281–322
6. Malinina, L., Patel, D. J., and Brown, R. E. (2017) How alphahelical motifs form functionally diverse lipid-binding compartments. *Annu. Rev. Biochem.* **86**, 609–636
7. Samygina, V. R., Popov, A. N., Cabo-Bilbao, A., Ochoa-Lizarralde, B., Goni-de-Cerio, F., Zhai, X., Molotkovsky, J. G., Patel, D. J., Brown, R. E., and Malinina, L. (2011) Enhanced selectivity for sulfatide by engineered human glycolipid transfer protein. *Structure.* **19**, 1644–1654
8. Samygina, V. R., Ochoa-Lizarralde, B., Popov, A. N., Cabo-Bilbao, A., Goni-de-Cerio, F., Molotkovsky, J. G., Patel, D. J., Brown, R. E., and Malinina, L. (2013) Structural insights into lipid-dependent reversible dimerization of human GLTP. *Acta Crystallogr. D Biol. Crystallogr.* **69**, 603–616
9. Kamlekar, R. K., Simanshu, D. K., Gao, Y. G., Kenoth, R., Pike, H. M., Prendergast, F. G., Malinina, L., Molotkovsky, J. G., Venyaminov, S. Y., Patel, D. J., and Brown, R. E. (2013) The glycolipid transfer protein (GLTP) domain of phosphoinositol 4-phosphate adaptor protein-2 (FAPP2): structure drives preference for simple neutral glycosphingolipids. *Biochim. Biophys. Acta.* **1831**, 417–427
10. Simanshu, D. K., Kamlekar, R. K., Wijesinghe, D. S., Zou, X., Zhai, X., Mishra, S. K., Molotkovsky, J. G., Malinina, L., Hinchcliffe, E. H., Chalfant, C. E., Brown, R. E., and Patel, D. J. (2013) Non-vesicular trafficking by a ceramide-1-phosphate transfer protein regulates eicosanoids. *Nature.* **500**, 463–467
11. Simanshu, D. K., Zhai, X., Munch, D., Hofius, D., Markham, J. E., Bielawski, J., Bielawska, A., Malinina, L., Molotkovsky, J. G., Mundy, J. W., Patel, D. J., and Brown, R. E. (2014) Arabidopsis accelerated cell death 11, ACD11, is a ceramide-1-phosphate transfer protein and intermediary regulator of phytoceramide levels. *Cell Rep.* **6**, 388–399
12. Ochoa-Lizarralde, B., Gao, Y. G., Popov, A. N., Samygina, V. R., Zhai, X., Mishra, S. K., Boldyrev, I. A., Molotkovsky, J. G., Simanshu, D. K., Patel, D. J., Brown, R. E., and Malinina, L. (2018) Structural analyses of 4-phosphate adaptor protein 2 yield mechanistic insights into sphingolipid recognition by the glycolipid transfer protein family. *J. Biol. Chem.* **293**, 16709–16723

≋ASBMB

13. Mattjus, P. (2016) Specificity of the mammalian glycolipid transfer proteins. *Chem. Phys. Lipids.* **194**, 72–78

14. Mishra, S. K., Gao, Y. G., Zou, X., Stephenson, D. J., Malinina, L., Hinchcliffe, E. H., Chalfant, C. E., and Brown, R. E. (2020) Emerging roles for human glycolipid transfer protein super-family members in the regulation of autophagy, inflammation, and cell death. *Prog. Lipid Res.* **78**, 101031

15. D'Angelo, G., Polishchuk, E., Di Tullio, G., Santoro, M., Di Campli, A., Godi, A., West, G., Bielawski, J., Chuang, C. C., van der Spoel, A. C., Platt, F. M., Hannun, Y. A., Polishchuk, R., Mattjus, P., and De Matteis, M. A. (2007) Glycosphingolipid synthesis requires FAPP2 transfer of glucosylceramide. *Nature.* **449**, 62–67

16. D'Angelo, G., Uemura, T., Chuang, C. C., Polishchuk, E., Santoro, M., Ohvo-Rekila, H., Sato, T., Di Tullio, G., Varriale, A., D'Auria, S., Daniele, T., Capuani, F., Johannes, L., Mattjus, P., Monti, M., *et al.* (2013) Vesicular and non-vesicular transport feed distinct glycosylation pathways in the Golgi. *Nature.* **501**, 116–120

17. Halter, D., Neumann, S., van Dijk, S. M., Wolthoorn, J., de Maziere, A. M., Vieira, O. V., Mattjus, P., Klumperman, J., van Meer, G., and Sprong, H. (2007) Pre- and post-Golgi translocation of glucosylceramide in glycosphingolipid synthesis. *J. Cell Biol.* **179**, 101–115

18. Yamaji, T., and Hanada, K. (2015) Sphingolipid metabolism and interorganellar transport: localization of sphingolipid enzymes and lipid transfer proteins. *Traffic.* **16**, 101–122

19. Kumagai, K., and Hanada, K. (2019) Structure, functions and regulation of CERT, a lipid-transfer protein for the delivery of ceramide at the ER-Golgi membrane contact sites. *FEBS Lett.* **593**, 2366–2377

20. Zhai, X., Gao, Y. G., Mishra, S. K., Simanshu, D. K., Boldyrev, I. A., Benson, L. M., Bergen 3rd, H. R., Malinina, L., Mundy, J., Molotkovsky, J. G., Patel, D. J., and Brown, R. E. (2017) Phosphatidylserine stimulates ceramide 1-phosphate (ClP) intermembrane transfer by ClP transfer proteins. *J. Biol. Chem.* **292**, 2531–2541

21. Gao, Y. G., Zhai, X., Boldyrev, I. A., Molotkovsky, J. G., Patel, D. J., Malinina, L., and Brown, R. E. (2021) Ceramide-1-phosphate transfer protein (CPTP) regulation by phosphoinositides. *J. Biol. Chem.* **296**, 100600

22. Mishra, S. K., Gao, Y. G., Deng, Y., Chalfant, C. E., Hinchcliffe, E. H., and Brown, R. E. (2018) CPTP: a sphingolipid transfer protein that regulates autophagy and inflammasome activation. *Autophagy.* **14**, 862–879

23. Mishra, S. K., Stephenson, D. J., Chalfant, C. E., and Brown, R. E. (2019) Upregulation of human glycolipid transfer protein (GLTP) induces necroptosis in colon carcinoma cells. *Biochim. Biophys. Acta Mol. Cell Biol. Lipids.* **1864**, 158–167

24. Yang, F., Guan, Y., Feng, X., Rolfs, A., Schluter, H., and Luo, J. (2019) Proteomics of the corpus callosum to identify novel factors involved in hypomyelinated Niemann-Pick Type C disease mice. *Mol. Brain.* **12**, 17

25. Khan, I., Katikaneni, D. S., Han, Q., Sanchez-Felipe, L., Hanada, K., Ambrose, R. L., Mackenzie, J. M., and Konan, K. V. (2014) Modulation of hepatitis C virus genome replication by glycosphingolipids and four-phosphate adaptor protein 2. *J. Virol.* **88**, 12276–12295

26. Lomize, A. L., Pogozheva, I. D., Lomize, M. A., and Mosberg, H. I. (2006) Positioning of proteins in membranes: a computational approach. *Protein Sci.* **15**, 1318–1333

27. Lomize, A. L., Pogozheva, I. D., and Mosberg, H. I. (2011) Anisotropic solvent model of the lipid bilayer. 2. Energetics of insertion of small molecules, peptides, and proteins in membranes. *J. Chem. Inf. Model.* **51**, 930–946

28. Lomize, M. A., Pogozheva, I. D., Joo, H., Mosberg, H. I., and Lomize, A. L. (2012) OPM database and PPM web server: resources for positioning of proteins in membranes. *Nucleic Acids Res.* **40**, D370–D376

29. Brooks, B. R., Brooks 3rd, C. L., Mackerell, A. D., Jr., Nilsson, L., Petrella, R. J., Roux, B., Won, Y., Archontis, G., Bartels, C., Boresch, S., Caflisch, A., Caves, L., Cui, Q., Dinner, A. R., Feig, M., *et al.* (2009) CHARMM: the biomolecular simulation program. *J. Comput. Chem.* **30**, 1545–1614

30. Jo, S., Kim, T., Iyer, V. G., and Im, W. (2008) CHARMM-GUI: a web-based graphical user interface for CHARMM. *J. Comput. Chem.* **29**, 1859–1865

31. Lee, J., Cheng, X., Swails, J. M., Yeom, M. S., Eastman, P. K., Lemkul, J. A., Wei, S., Buckner, J., Jeong, J. C., Qi, Y., Jo, S., Pande, V. S., Case, D. A., Brooks 3rd, C. L., MacKerell, A. D., Jr., *et al.* (2016) CHARMM-GUI input generator for NAMD, GROMACS, AMBER, OpenMM, and CHARMM/OpenMM simulations using the CHARMM36 additive force field. *J. Chem. Theory Comput.* **12**, 405–413

32. Wu, E. L., Cheng, X., Jo, S., Rui, H., Song, K. C., Davila-Contreras, E. M., Qi, Y., Lee, J., Monje-Galvan, V., Venable, R. M., Klauda, J. B., and Im, W. (2014) CHARMM-GUI membrane builder toward realistic biological membrane simulations. *J. Comput. Chem.* **35**, 1997–2004

33. Jorgensen, W. L., Chandrasekhar, J., Madura, J. D., Impey, R. W., and Klein, M. L. (1983) Comparison of simple potential functions for simulating liquid water. *J. Chem. Phys.* **79**, 926–935

34. Kučerka, N., Tristram-Nagle, S., and Nagle, J. F. (2005) Structure of fully hydrated fluid phase lipid bilayers with mono-unsaturated chains. *J. Membr. Biol.* **208**, 193–202

35. Kučerka, N., Nagle, J. F., Sachs, J. N., Feller, S. E., Pencer, J., Jackson, A., and Katsaras, J. (2008) Lipid bilayer structure determined by the simultaneous analysis of neutron and X-ray scattering data. *Biophys. J.* **95**, 2356–2367

36. Phillips, J. C., Hardy, D. J., Maia, J. D. C., Stone, J. E., Ribeiro, J. V., Bernardi, R. C., Buch, R., Fiorin, G., Henin, J., Jiang, W., McGreevy, R., Melo, M. C. R., Radak, B. K., Skeel, R. D., Singharoy, A., *et al.* (2020) Scalable molecular dynamics on CPU and GPU architectures with NAMD. *J. Chem. Phys.* **153**, 044130

37. Huang, J., Rauscher, S., Nawrocki, G., Ran, T., Feig, M., de Groot, B. L., Grubmuller, H., and MacKerell, A. D., Jr. (2017) CHARMM36m: an improved force field for folded and intrinsically disordered proteins. *Nat. Methods.* **14**, 71–73

38. Nose, S. (1984) A unified formulation of the constant temperature molecular-dynamics methods. *J. Chem. Phys.* **81**, 511–519

39. Hoover, W. G. (1985) Canonical dynamics: equilibrium phase-space distributions. *Phys. Rev. A Gen. Phys.* **31**, 1695–1697

40. Humphrey, W., Dalke, A., and Schulten, K. (1996) VMD: visual molecular dynamics. *J. Mol. Graph.* **14**, 27–38

41. Tubiana, T., Carvaillo, J. C., Boulard, Y., and Bressanelli, S. (2018) TTClust: a versatile molecular simulation trajectory clustering program with graphical summaries. *J. Chem. Inf. Model.* **58**, 2178–2182

42. Salentin, S., Schreiber, S., Haupt, V. J., Adasme, M. F., and Schroeder, M. (2015) PLIP: fully automated protein-ligand interaction profiler. *Nucleic Acids Res.* **43**, W443–W447

43. Rao, C. S., Lin, X., Pike, H. M., Molotkovsky, J. G., and Brown, R. E. (2004) Glycolipid transfer protein mediated transfer of glycosphingolipids between membranes: a model for action based on kinetic and thermodynamic analyses. *Biochemistry.* **43**, 13805–13815

44. Rao, C. S., Chung, T., Pike, H. M., and Brown, R. E. (2005) Glycolipid transfer protein interaction with bilayer vesicles: modulation by changing lipid composition. *Biophys. J.* **89**, 4017–4028

45. West, G., Nylund, M., Peter Slotte, J., and Mattjus, P. (2006) Membrane interaction and activity of the glycolipid transfer protein. *Biochim. Biophys. Acta.* **1758**, 1732–1742

46. Neumann, S., Opacic, M., Wechselberger, R. W., Sprong, H., and Egmond, M. R. (2008) Glycolipid transfer protein: clear structure and activity, but enigmatic function. *Adv. Enzyme Regul.* **48**, 137–151

47. Zhai, X., Malakhova, M. L., Pike, H. M., Benson, L. M., Bergen 3rd, H. R., Sugar, I. P., Malinina, L., Patel, D. J., and Brown, R. E. (2009) Glycolipid acquisition by human glycolipid transfer protein dramatically alters intrinsic tryptophan fluorescence: insights into glycolipid binding affinity. *J. Biol. Chem.* **284**, 13620–13628

48. Mattjus, P. (2009) Glycolipid transfer proteins and membrane interaction. *Biochim. Biophys. Acta.* **1788**, 267–272

49. Kamlekar, R. K., Gao, Y., Kenoth, R., Molotkovsky, J. G., Prendergast, F. G., Malinina, L., Patel, D. J., Wessels, W. S., Venyaminov, S. Y., and Brown, R. E. (2010) Human GLTP: three distinct functions for the three tryptophans in a novel peripheral amphitropic fold. *Biophys. J.* **99**, 2626–2635

50. Ohvo-Rekila, H., and Mattjus, P. (2011) Monitoring glycolipid transfer protein activity and membrane interaction with the surface plasmon resonance technique. *Biochim. Biophys. Acta.* **1808**, 47–54

51. Zou, X., Chung, T., Lin, X., Malakhova, M. L., Pike, H. M., and Brown, R. E. (2008) Human glycolipid transfer protein (GLTP) genes: organization, transcriptional status and evolution. *BMC Genomics.* **9**, 72

52. Mattjus, P., Turcq, B., Pike, H. M., Molotkovsky, J. G., and Brown, R. E. (2003) Glycolipid intermembrane transfer is accelerated by HET-C2, a filamentous fungus gene product involved in the cell-cell incompatibility response. *Biochemistry.* **42**, 535–542

53. Kenoth, R., Simanshu, D. K., Kamlekar, R. K., Pike, H. M., Molotkovsky, J. G., Benson, L. M., Bergen 3rd, H. R., Prendergast, F. G., Malinina, L., Venyaminov, S. Y., Patel, D. J., and Brown, R. E. (2010) Structural determination and tryptophan fluorescence of heterokaryon incompatibility C2 protein (HET-C2), a fungal glycolipid transfer protein (GLTP), provide novel insights into glycolipid specificity and membrane interaction by the GLTP fold. *J. Biol. Chem.* **285**, 13066–13078

54. Kenoth, R., Kamlekar, R. K., Simanshu, D. K., Gao, Y., Malinina, L., Prendergast, F. G., Molotkovsky, J. G., Patel, D. J., Venyaminov, S. Y., and Brown, R. E. (2011) Conformational folding and stability of the HET-C2 glycolipid transfer protein fold: does a molten globule-like state regulate activity? *Biochemistry.* **50**, 5163–5171

55. D'Angelo, G., Rega, L. R., and De Matteis, M. A. (2012) Connecting vesicular transport with lipid synthesis: FAPP2. *Biochim. Biophys. Acta.* **1821**, 1089–1095

56. Brodersen, P., Petersen, M., Pike, H. M., Olszak, B., Skov, S., Odum, N., Jorgensen, L. B., Brown, R. E., and Mundy, J. (2002) Knockout of Arabidopsis accelerated-cell-death11 encoding a sphingosine transfer protein causes activation of programmed cell death and defense. *Genes Dev.* **16**, 490–502

57. Petersen, N. H., McKinney, L. V., Pike, H., Hofius, D., Zakaria, A., Brodersen, P., Petersen, M., Brown, R. E., and Mundy, J. (2008) Human GLTP and mutant forms of ACD11 suppress cell death in the Arabidopsis acd11 mutant. *FEBS J.* **275**, 4378–4388

58. Moqadam, M., Tubiana, T., Moutoussamy, E. E., and Reuter, N. (2021) Membrane models for molecular simulations of peripheral membrane proteins. *Adv. Phys. X.* **6**, 1

59. Sommer, B. (2013) Membrane packing problems: a short review on computational membrane modeling methods and tools. *Comp. Struct. Biotech.* **5**, e201302014

60. Moradi, S., Nowroozi, A., and Shahlaei, M. (2019) Shedding light on the structural properties of lipid bilayers using molecular dynamics simulation: a review study. *RSC Adv.* **9**, 4644

61. Manni, M. M., Tiberti, M. L., Pagnotta, S., Barelli, H., Gautier, R., and Antonny, B. (2018) Acyl chain asymmetry and polyunsaturation of brain phospholipids facilitate membrane vesiculation without leakage. *Elife.* **7**, e34394

62. Nylund, M., Fortelius, C., Palonen, E. K., Molotkovsky, J. G., and Mattjus, P. (2007) Membrane curvature effects on glycolipid transfer protein activity. *Langmuir.* **23**, 11726–11733

63. Zhai, X., Momsen, W. E., Malakhov, D. A., Boldyrev, I. A., Momsen, M. M., Molotkovsky, J. G., Brockman, H. L., and Brown, R. E. (2013) GLTP-fold interaction with planar phosphatidylcholine surfaces is synergistically stimulated by phosphatidic acid and phosphatidylethanolamine. *J. Lipid Res.* **54**, 1103–1113

64. Nazeer, M., Waheed, H., Saeed, M., Ali, S. Y., Choudhary, M. I., Ul-Haq, Z., and Ahmed, A. (2019) Purification and characterization of a nonspecific lipid transfer protein 1 (nsLTP1) from Ajwain (Trachyspermum ammi) seeds. *Sci. Rep.* **9**, 4148

65. Madni, Z. K., Tripathi, S. K., and Salunke, D. M. (2020) Structural insights into the lipid transfer mechanism of a non-specific lipid transfer protein. *Plant J.* **102**, 340–352

66. Shi, Z., Wang, Z. J., Xu, H. L., Tian, Y., Li, X., Bao, J. K., Sun, S. R., and Yue, B. S. (2013) Modeling, docking and dynamics simulations of a non-specific lipid transfer protein from Peganum harmala L. *Comput. Biol. Chem.* **47**, 56–65

67. Hunter, N. H., Bakula, B. C., and Bruce, C. D. (2018) Molecular dynamics simulations of apo and holo forms of fatty acid binding protein 5 and cellular retinoic acid binding protein II reveal highly mobile protein, retinoic acid ligand, and water molecules. *J. Biomol. Struct. Dyn.* **36**, 1893–1907

68. Guo, Y., Duan, M., and Yang, M. (2019) The observation of ligand-binding-relevant open states of fatty acid binding protein by molecular dynamics simulations and a Markov state model. *Int. J. Mol. Sci.* **20**, 3476

69. Long, D., Mu, Y., and Yang, D. (2009) Molecular dynamics simulation of ligand dissociation from liver fatty acid binding protein. *PLoS One.* **4**, e6081

70. Ryan, M. M., Temple, B. R., Phillips, S. E., and Bankaitis, V. A. (2007) Conformational dynamics of the major yeast phosphatidylinositol transfer protein sec14p: insight into the mechanisms of phospholipid exchange and diseases of sec14p-like protein deficiencies. *Mol. Biol. Cell.* **18**, 1928–1942

71. Grabon, A., Orlowski, A., Tripathi, A., Vuorio, J., Javanainen, M., Rog, T., Lonnfors, M., McDermott, M. I., Siebert, G., Somerharju, P., Vattulainen, I., and Bankaitis, V. A. (2017) Dynamics and energetics of the mammalian phosphatidylinositol transfer protein phospholipid exchange cycle. *J. Biol. Chem.* **292**, 14438–14455

72. Nylund, M., and Mattjus, P. (2005) Protein mediated glycolipid transfer is inhibited FROM sphingomyelin membranes but enhanced TO sphingomyelin containing raft like membranes. *Biochim. Biophys. Acta.* **1669**, 87–94

73. Wiener, M. C., and White, S. H. (1992) Structure of a fluid dioleoylphosphatidylcholine bilayer determined by joint refinement of x-ray and neutron diffraction data. III. Complete structure. *Biophys. J.* **61**, 434–447

74. Jiang, T., Yu, K., Hartzell, H. C., and Tajkhorshid, E. (2017) Lipids and ions traverse the membrane by the same physical pathway in the nhTMEM16 scramblase. *Elife.* **6**, e28671

75. Pomorski, T. G., and Menon, A. K. (2016) Lipid somersaults: uncovering the mechanisms of protein-mediated lipid flipping. *Prog. Lipid Res.* **64**, 69–84

76. Perez, C., Gerber, S., Boilevin, J., Bucher, M., Darbre, T., Aebi, M., Reymond, J. L., and Locher, K. P. (2015) Structure and mechanism of an active lipid-linked oligosaccharide flippase. *Nature.* **524**, 433–438

ASBMB